Nanoscale

PAPER

View Article Online
View Journal | View Issue

Cite this: *Nanoscale*, 2024, **16**, 13687

Electrically tunable non-radiative lifetime in WS_2/WSe_2 heterostructures†

Anran Wang,[a] Xingguang Wu,[b] Siwen Zhao,[b] Zheng Vitto Han,[c] Yi Shi,[a] Giulio Cerullo[d,e] and Fengqiu Wang *[a]

Received 8th May 2024,
Accepted 18th June 2024

DOI: 10.1039/d4nr01982b

rsc.li/nanoscale

Van der Waals heterostructures based on transition metal dichalcogenides (TMDs) have emerged as excellent candidates for next-generation optoelectronics and valleytronics, due to their fascinating physical properties. The understanding and active control of the relaxation dynamics of heterostructures play a crucial role in device design and optimization. Here, we investigate the back-gate modulation of exciton dynamics in a WS_2/WSe_2 heterostructure by combining time-resolved photoluminescence (TRPL) and transient absorption spectroscopy (TAS) at cryogenic temperatures. We find that the non-radiative relaxation lifetimes of photocarriers in heterostructures can be electrically controlled for samples with different twist-angles, whereas such lifetime tuning is not present in standalone monolayers. We attribute such an observation to doping-controlled competition between interlayer and intralayer recombination pathways in high-quality WS_2/WSe_2 samples. The simultaneous measurement of TRPL and TAS lifetimes within the same sample provides additional insight into the influence of coexisting excitons and background carriers on the photo-response, and points to the potential of tailoring light–matter interactions in TMD heterostructures.

Introduction

Over the last decade, there has been remarkable progress in exploring the new physical properties of transition metal dichalcogenides (TMDs), a material platform ideal for studying valleytronics and realizing novel optoelectronic functionalities.[1–3] The attractive Coulomb interactions and the reduced screening effect in a two-dimensional environment result in the formation of tightly bound excitons with large binding energy, which dominate the optical properties of TMDs.[3,4] Vertically stacked van der Waals (vdW) heterostructures based on TMDs exhibit diverse and extraordinary characteristics not present in monolayers, such as the presence of interlayer excitons, twist-angle dependent moiré superlattices, modified optical selection rules and strong correlation effects.[5–10] Benefiting from the spatial separation of the Coulomb-bound electron–hole residing in different layers, interlayer excitons display long valley lifetimes due to reduced exchange interactions and suppressed intervalley scattering.[5,11] The manipulation of excitonic states in vdW heterostructures *via* various strategies has been proposed, including externally applied electric or magnetic fields and the introduction of a moiré superlattice.[12–17]

To probe still further the fundamental exciton physics and explore potential applications of vdW heterostructures, population as well as valley-polarization relaxation dynamics have been widely investigated by time-resolved techniques.[18] It is well known that the intralayer exciton lifetime in monolayer TMDs is as short as a few to tens of picoseconds at low temperature.[19–21] Compared with the fast relaxation of intralayer excitons, the radiative lifetime of an interlayer exciton as measured by time-resolved photoluminescence (TRPL) is several orders of magnitude longer, and has shown the desirable feature of electrical tunability.[5,13–15,22–24] For example, by tuning the electric field applied to the heterostructure, the interlayer exciton lifetime in MoS_2/WS_2 can be tuned from 100 ns to 400 ns.[16] Despite these advances, a general overview of the intra- and inter-layer photocarrier dynamics and its associated radiative and non-radiative decay channels is yet to be fully established. In particular, it has been shown recently that the optical behaviors of intralayer excitons in $MoSe_2/MoS_2$ and WS_2/WSe_2 heterostructures differ appreciably from those of

[a]School of Electronic Science and Engineering, Nanjing University, Nanjing 210093, China. E-mail: fwang@nju.edu.cn
[b]Shenyang National Laboratory for Materials Science, Institute of Metal Research, Chinese Academy of Sciences, Shenyang 110016, China
[c]State Key Laboratory of Quantum Optics and Quantum Optics Devices, Institute of Opto-Electronics, Shanxi University, Taiyuan 030006, China
[d]Dipartimento di Fisica, Politecnico di Milano, Piazza Leonardo da Vinci 32, I-20133 Milano, Italy
[e]Istituto di Fotonica e Nanotecnologie (IFN), CNR, Piazza Leonardo da Vinci 32, I-20133 Milano, Italy

† Electronic supplementary information (ESI) available. See DOI: https://doi.org/10.1039/d4nr01982b

the monolayers, suggesting contributions from many-body effects and moiré potential in heterostructures.[25–29] While the photoluminescence (PL) of intralayer excitons in heterostructures has been widely studied and shows electrical tunability,[27–29] the non-radiative recombination dynamics in the heterostructures has scarcely been investigated. Some existing transient absorption spectroscopy (TAS) studies mostly focus on the charge transfer and exciton formation process.[26,30–32]

In this work, we have fabricated a back-gated field-effect transistor based on a hexagonal boron nitride (h-BN) encapsulated WS_2/WSe_2 heterostructure with few-layer graphene back-gate and contact electrodes, where radiative and non-radiative properties of excitons at low temperature can be systematically investigated at different doping levels. We first studied the carrier concentration dependent steady-state PL and reflection contrast spectra of excitons in the WS_2/WSe_2 heterostructure, and clearly identified the static optical features of neutral and charged excitons. For the samples we studied, both radiative and non-radiative transient dynamics at the WS_2 and WSe_2 resonances exhibit significant electrostatic doping dependence. In particular, the non-radiative relaxation dynamics of photocarriers in the heterostructure shows a unique and strong back-gate voltage dependence, which is not observed in standalone monolayers. The dynamics can be well explained by gate-controlled interfacial potential differences at the heterostructure. Our results highlight the influence of the doping level introduced by the back gate on the recombination of excitonic states in the heterostructure and provide new insight into the optical behaviors of excitonic states in TMD heterostructures.

Results and discussion

Fig. 1a shows an optical microscopy image of a representative WS_2/WSe_2 heterostructure device, and the side-view of the device is schematically illustrated in Fig. 1b. The WS_2 and WSe_2 monolayers were fabricated by mechanical exfoliation and then encapsulated in two hexagonal boron nitride (h-BN) flakes by a dry transfer technique on a 285 nm SiO_2/Si substrate. The top and bottom h-BN flakes were used to mitigate the influence of surface defects and charged impurities. The carrier concentration of the WS_2/WSe_2 heterostructure can be efficiently gated by the few-layer graphene electrodes, and the bottom h-BN serves as the gate dielectric of the device. A schematic illustration of the type-II band alignment of the WS_2/WSe_2 heterostructure is shown in Fig. 1c, where the electrons tend to reside in the WS_2 layer while the holes prefer to stay in the WSe_2 layer.

Gate-dependent PL spectra in the heterostructure were characterized under a cryogenic temperature (~7 K), as shown in Fig. 2a. The excitation energy was fixed at ~2.33 eV (532 nm) so that both WS_2 and WSe_2 monolayers can be excited. Without applying any back-gate voltage, the emission from neutral intralayer excitons dominates the PL spectra. When a positive (negative) back-gate voltage is applied, the negatively (positively) charged exciton with an additional electron (hole) will appear in the PL spectra, and dominates the PL spectra with increasing back-gate voltages. It is noticed that the PL intensity of the negative charged excitons slightly redshifts as the applied voltage increases at a high doping level. This nontrivial doping dependence of the trion emission can be attributed to the combined effects of the restricted scattering phase space and the electrostatic screening effect.[21,33]

To further study the carrier concentration dependence of the optical transitions in the WS_2/WSe_2 heterostructure, the gate-dependent reflection contrast spectrum under cryogenic temperature was also measured, and the results are summarized in Fig. 2b. For the heterostructure without the back-gate voltage, two prominent features around 1.68 eV and 2.00 eV can be observed, corresponding to the A exciton resonance of WSe_2 and WS_2, respectively. It can be seen that the exciton resonances for the two different layers have different back-gate dependencies. When the back-gate voltage varies from −2 V to 2 V, both A exciton resonances of WS_2 and WSe_2 are present, suggesting that the Fermi level is within the band energy gap of the two layers. For large positive back-gate voltages, electron-doping strongly suppresses the A exciton resonance in WS_2. Meanwhile, only a slight red shift occurs in the A exciton of WSe_2. Similarly, for large negative back-gate voltages, only the resonance from WSe_2 is seen to vanish due to hole doping,

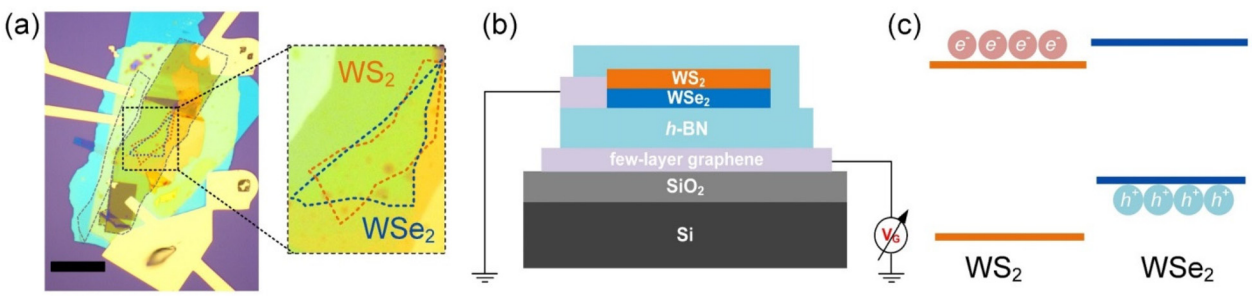

Fig. 1 (a) Optical microscopy image of the WS_2/WSe_2 heterostructure; orange and blue dashed lines mark the boundaries of monolayer WS_2 and WSe_2 regions, respectively. Gray dashed boxes mark the few-layer graphene electrodes. The scale bar is 20 μm. (b) Side-view illustration of the back-gated heterostructure device. (c) Schematic illustration of the type-II band alignment of the WS_2/WSe_2 heterostructure.

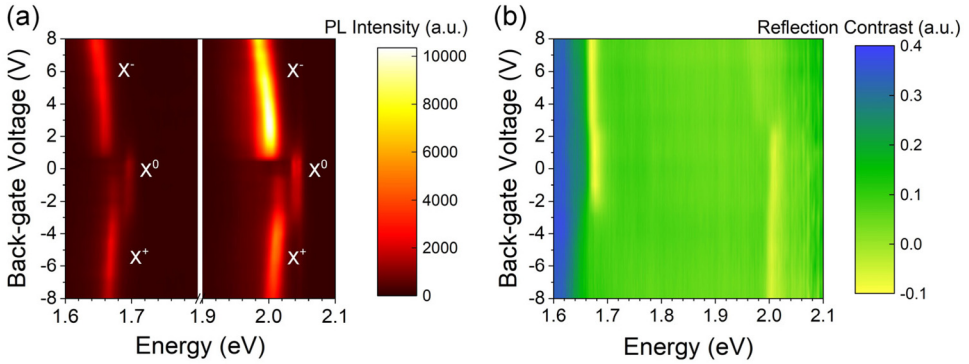

Fig. 2 (a) Back-gate-voltage-dependent PL and (b) reflection contrast spectra of the WS_2/WSe_2 heterostructure at 7 K.

and the exciton response of WS_2 remains unaffected. The peculiar back-gate dependence of PL and reflection contrast spectra is consistent with the type-II band alignment of the heterostructure. It has been observed before and is attributed to the signature of the large twist-angle in the WS_2/WSe_2 heterostructure.[34] The significant change of emission and reflection spectra at intralayer exciton resonances (including neutral and charged exciton) means the electrostatic doping-level in the heterostructure can be effectively modulated by the graphene back-gate. A heterostructure with a small twist-angle was also investigated, and the results are presented in the ESI.†

As is shown in Fig. 3a, the heterostructure sample does not exhibit PL emission from interlayer exciton, due to the large twist-angle induced momentum mismatch.[34,35] We therefore focused our investigation on intralayer exciton resonances in the WS_2/WSe_2 heterostructure. TRPL measurements were carried out using a 10 ps excitation laser at a wavelength of 532 nm (~2.33 eV). The emission signal was detected using a Becker & Hickl GmbH hybrid single-photon detector with a time-correlated single photon counting module. A monochromator was placed in front of the single-photon detector to select the emission wavelength. PL lifetimes were extracted from the mono-exponential deconvolution of the measured data with the instrumental response function (IRF), which had a 55 ps full width at half maximum (FWHM) duration. Interestingly, the PL measured at the WSe_2 resonance (~1.68 eV) as shown in Fig. 3b exhibits a quite long lifetime and shows a clear gate-voltage dependence, with the longest lifetime (~244 ps) obtained at back-gate voltages corresponding to the charge-neutrality region. The WS_2 resonance shows similar results but with a significantly shorter time constant, as shown in ESI Fig. S1.† We present the change of PL lifetimes with back-gate voltages at ~1.68 eV in Fig. 3c, and the time constants extend from ~80 ps to ~250 ps. To verify whether such an observation is intrinsic to monolayers, we performed the same TRPL measurement on a monolayer WSe_2 area from the heterostructure. The results are shown in Fig. 3d and e. Though the measurements of lifetimes with a positive back-gate voltage are probably limited by IRF, two clear differences can still be seen. First, the lifetime of the intralayer exciton in the monolayer is much shortened, with the longest lifetime recorded at ~98 ps (charge-neutrality region). Second, although gate voltage dependence is still present in the monolayer, the decay times at positive and negative voltages are almost converged to constant values.

While previous works have attributed the gate-dependence of lifetime in the monolayer to the switching of excitonic species, such as the change from neutral excitons to charged excitons,[21,36] there is little prior experimental work that can be drawn on to explain the gate-tunable photocarrier dynamics at intralayer resonances in the heterostructure. The different shape of the modulation curves in Fig. 3c and e also suggests different underlying mechanisms. In fact, the exciton lifetimes measured by the TRPL technique are fundamentally impacted by both radiative and non-radiative recombination pathways. Therefore, simultaneously probing the non-radiative lifetimes of intralayer excitons using ultrafast TAS may provide important new insights and help elaborate the overall physical picture of the photocarrier recombination in the heterostructure.

To understand the difference in PL lifetimes of intralayer excitons between the WS_2/WSe_2 heterostructure and monolayer WSe_2, we performed ultrafast transient reflectance measurements. Here, we selected a pump wavelength of 655 nm (~1.89 eV) provided by a picosecond diode laser with a pulse duration of ~190 ps, so that monolayer WSe_2 was selectively photo-excited. The probe pulse was provided by a picosecond supercontinuum light source connected to an acoustic-optical modulator (AOM). The synchronization and time-delay between the picosecond diode laser and the AOM were controlled using two custom-made frequency and time-delay control boards, and details of the ultrafast pump–probe experimental setup can be found in ref. 37. The probe energy was fixed at ~1.68 eV, aligned with the A exciton resonance of WSe_2. An IRF of ~0.2 ns can be deduced by the FWHM of the convolution of pump and probe pulses. As is shown in Fig. 4a, the decay time of photocarriers in the heterostructure is ~1472 ± 29 ps at 7 K, which is notably longer than that in monolayer WSe_2 (~678 ± 11 ps). The prolonged lifetime in the WS_2/WSe_2

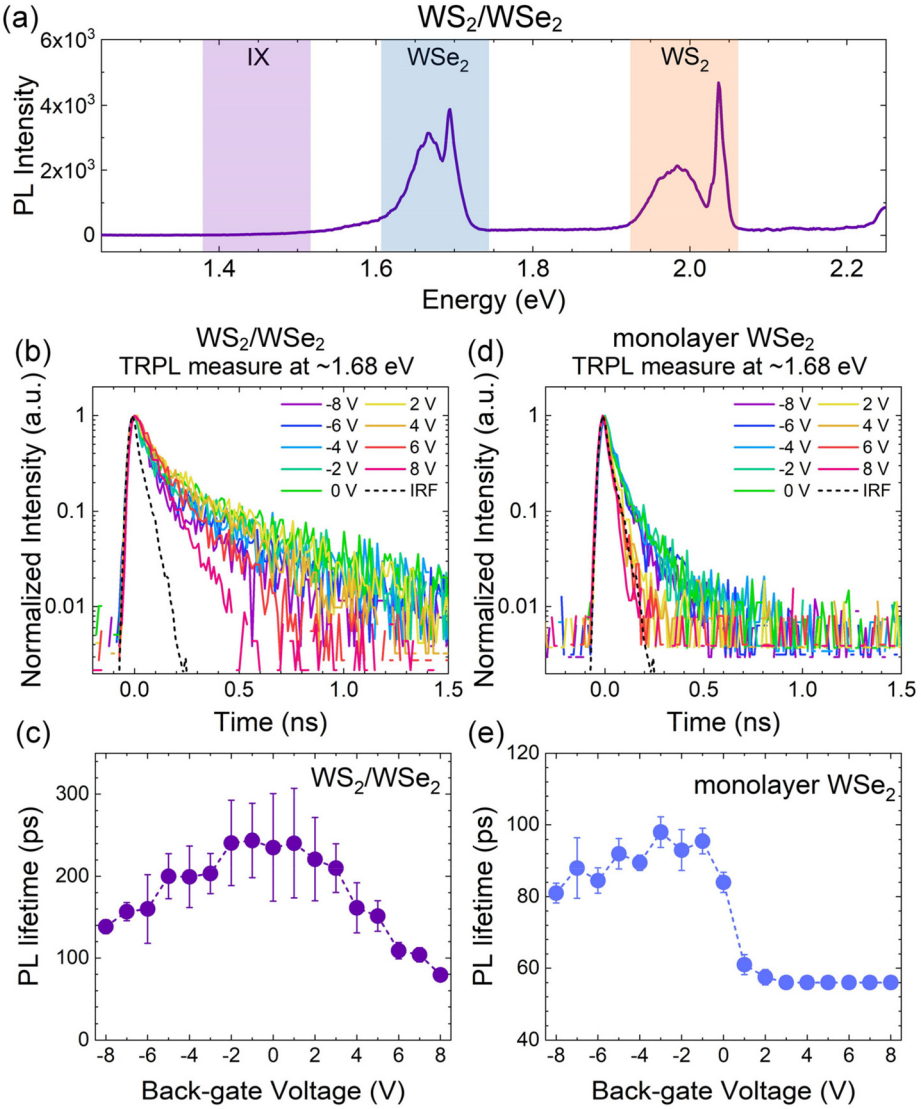

Fig. 3 (a) Photoluminescence spectrum of the WS_2/WSe_2 heterostructure without back-gate voltage. The orange, blue and purple stripes are visual guides marking the emission peak positions of WS_2, WSe_2 and interlayer excitons (IX), respectively. Normalized time-resolved PL results of (b) the WS_2/WSe_2 heterostructure and (d) monolayer WSe_2 at WSe_2 resonant energy (~1.68 eV) under different back-gate voltages. The black dashed line represents the IRF for the TRPL setup. PL lifetimes extracted from the TRPL measurements of (c) the WS_2/WSe_2 heterostructure and (e) monolayer WSe_2 as a function of the back-gate voltage. All the measurements were performed at 7 K.

heterostructure can be easily understood. For the heterostructure, the photogenerated electrons in WSe_2 will rapidly transfer to the conduction band of WS_2 on a timescale of a few hundred femtoseconds,[38] while the photogenerated holes still remain in the valence band of WSe_2. Under such a scenario, the relatively slow interlayer recombination dominates. The PL lifetime measured with TRPL experiments, $\tau_{lifetime}$, can be described using the following equation: $1/\tau_{lifetime} = 1/\tau_{rad} + 1/\tau_{non\text{-}rad}$, where τ_{rad} and $\tau_{non\text{-}rad}$ represent the radiative and non-radiative lifetimes of the photocarriers, respectively. Clearly, the appreciably longer non-radiative lifetime of photogenerated carriers in the WS_2/WSe_2 heterostructure as shown in Fig. 4a can well account for the observed elongation of PL lifetimes for excitons shown in Fig. 3.

Then, the dependence of non-radiative lifetime (by TAS) on the electrostatic doping level was studied with the back-gate voltage varying from −8 V to 8 V. Fig. 4b shows the normalized TAS curves and fitting results for monolayer WSe_2. It can be seen that the relaxation dynamics of intralayer excitons is not affected by the back-gate voltage, and the non-radiative lifetime in the monolayer is around 700 picoseconds. ESI Table S1† presents the fitting results of TAS lifetimes for monolayer WSe_2 and the WS_2/WSe_2 heterostructure. The independence from background carrier concentration in monolayer WSe_2 indicates that the different PL lifetimes for positive and negative back-gate voltages (Fig. 3d and e) are probably due to the switching of excitonic species. Interestingly, the non-radiative lifetimes in the WS_2/WSe_2 heterostructures exhibit sub-

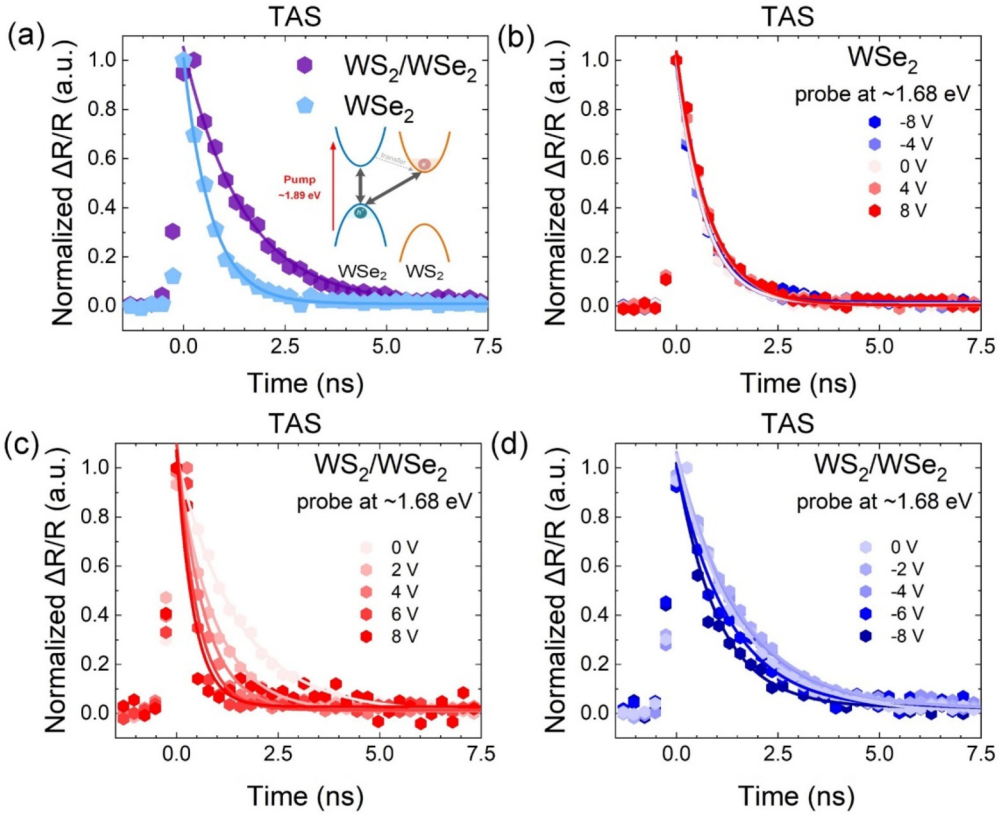

Fig. 4 (a) Normalized transient reflectance of the WS_2/WSe_2 heterostructure and monolayer WSe_2 without back-gate voltage. Inset: the schematic illustration of the type-II band alignment in the WS_2/WSe_2 heterostructure. (b) Transient reflectance of monolayer WSe_2 under V_{BG} varying from −8 V to 8 V. The transient reflectance of the WS_2/WSe_2 heterostructure (c) under back-gate voltages varying from 0 V to 8 V and (d) under back-gate voltages varying from −8 V to 0 V. All the measurements were performed at 7 K.

stantial gate dependence, as shown in Fig. 4c and d. The non-radiative dynamics probed at different back-gate voltages shows that the decay time under electrical neutrality conditions is much longer than that when electron or hole doping is introduced. As is shown in Fig. 4c, the lifetime dramatically decreases from ~1472 ± 29 ps to ~422 ± 41 ps for heavy electron doping (V_{BG} = 8 V). Similarly, when the back-gate voltage was tuned to negative, the lifetime also decreased with the increase of the hole doping concentration, and the shortest decay time at −8 V is ~1023 ± 59 ps. We subsequently tuned the probe energy across the A-exciton resonance range of WSe_2, and the same back-gate voltage dependence is observed (as shown in ESI Fig. S2†). The faster TAS lifetime at V_{BG} = 8 V (~422 ps) compared with that of the monolayer (~700 ps) indicates that the recombination of photocarriers in heterostructures is probably influenced by other factors, such as many-body effects and band alignment offset shift introduced by the back-gate.[29]

As for the observed gate-dependent TAS lifetimes, the experimental results can be explained by the doping-controllable competition of interlayer and intralayer recombination pathways. In the charge-neutrality region, the relatively slow interlayer recombination of photocarriers dominates, leading to prolonged lifetimes. However, when electrostatic doping is introduced in the WS_2/WSe_2 heterostructure, the occupation of the WS_2 conduction band or the WSe_2 valence band reduces the energy difference between the two constituent monolayers. As a result, charge transfer is less efficient and intralayer rather than interlayer recombination becomes the dominant relaxation channel of photocarriers in the case of heavy doping. Taking into account the smaller energy difference in conduction bands between WS_2 and WSe_2, the intralayer recombination pathways are expected to be more effective with n-doping, in agreement with the shorter non-radiative lifetimes observed under positive back-gate voltages. Furthermore, we ruled out the potential effects of exciton–exciton annihilation as the dynamics showed negligible density dependence in our experiments, as shown in ESI Fig. S3.† The signatures of electrically tunable lifetimes of near-aligned WS_2/WSe_2 heterostructures can be obtained from ESI Fig. S4,† suggesting independence from twist-angles.

Conclusions

In summary, we have carried out detailed lifetime measurements on a WS_2/WSe_2 heterostructure at a cryogenic temperature, combining time-resolved fluorescence and transient

absorption spectroscopy. Both radiative and non-radiative dynamics exhibit clear gate-voltage dependent behaviour. Fascinatingly, the non-radiative relaxation dynamics can be effectively back-gate-tuned in heterostructures, but not in monolayers. We attribute the pronounced gate-dependence to the competition between coexisting interlayer and intralayer recombination channels, where doping the heterostructure proves to be an effective knob for changing the intra and cross-layer occupation of photocarriers. Our results pinpoint a new way to electrically control the optoelectronic properties of TMD heterostructures, and help further elucidate the relatively complex relaxation dynamics of excitons and photocarriers in van der Waals heterostructures.

Data availability

The data supporting the findings presented in this study are not publicly available at this time, but may be obtained from the corresponding author upon reasonable request.

Conflicts of interest

There are no conflicts of interest to declare.

Acknowledgements

This work was supported in part by the National Key Research and Development Program of China (2022YFA1204303).

References

1 K. S. Novoselov, A. Mishchenko, A. Carvalho and A. H. Castro Neto, *Science*, 2016, **353**, aac9439.
2 J. R. Schaibley, H. Yu, G. Clark, P. Rivera, J. S. Ross, K. L. Seyler, W. Yao and X. Xu, *Nat. Rev. Mater.*, 2016, **1**, 16055.
3 E. C. Regan, D. Wang, E. Y. Paik, Y. Zeng, L. Zhang, J. Zhu, A. H. MacDonald, H. Deng and F. Wang, *Nat. Rev. Mater.*, 2022, **7**, 778–795.
4 D. Y. Qiu, F. H. da Jornada and S. G. Louie, *Phys. Rev. Lett.*, 2013, **111**, 216805.
5 P. Rivera, J. R. Schaibley, A. M. Jones, J. S. Ross, S. Wu, G. Aivazian, P. Klement, K. Seyler, G. Clark, N. J. Ghimire, J. Yan, D. G. Mandrus, W. Yao and X. Xu, *Nat. Commun.*, 2015, **6**, 6242.
6 E. M. Alexeev, D. A. Ruiz-Tijerina, M. Danovich, M. J. Hamer, D. J. Terry, P. K. Nayak, S. Ahn, S. Pak, J. Lee, J. I. Sohn, M. R. Molas, M. Koperski, K. Watanabe, T. Taniguchi, K. S. Novoselov, R. V. Gorbachev, H. S. Shin, V. I. Fal'ko and A. I. Tartakovskii, *Nature*, 2019, **567**, 81–86.
7 C. Jin, E. C. Regan, A. Yan, M. Iqbal Bakti Utama, D. Wang, S. Zhao, Y. Qin, S. Yang, Z. Zheng, S. Shi, K. Watanabe, T. Taniguchi, S. Tongay, A. Zettl and F. Wang, *Nature*, 2019, **567**, 76–80.
8 A. Ciarrocchi, D. Unuchek, A. Avsar, K. Watanabe, T. Taniguchi and A. Kis, *Nat. Photonics*, 2019, **13**, 131–136.
9 E. C. Regan, D. Wang, C. Jin, M. I. B. Utama, B. Gao, X. Wei, S. Zhao, W. Zhao, Z. Zhang, K. Yumigeta, M. Blei, J. D. Carlström, K. Watanabe, T. Taniguchi, S. Tongay, M. Crommie, A. Zettl and F. Wang, *Nature*, 2020, **579**, 359–363.
10 Y. Xu, S. Liu, D. A. Rhodes, K. Watanabe, T. Taniguchi, J. Hone, V. Elser, K. F. Mak and J. Shan, *Nature*, 2020, **587**, 214–218.
11 J. S. Ross, P. Rivera, J. Schaibley, E. Lee-Wong, H. Yu, T. Taniguchi, K. Watanabe, J. Yan, D. Mandrus, D. Cobden, W. Yao and X. Xu, *Nano Lett.*, 2017, **17**, 638–643.
12 O. Karni, E. Barré, S. C. Lau, R. Gillen, E. Y. Ma, B. Kim, K. Watanabe, T. Taniguchi, J. Maultzsch, K. Barmak, R. H. Page and T. F. Heinz, *Phys. Rev. Lett.*, 2019, **123**, 247402.
13 L. Zhang, R. Gogna, G. William Burg, J. Horng, E. Paik, Y. Chou, K. Kim, E. Tutuc and H. Deng, *Phys. Rev. B*, 2019, **100**, 041402.
14 P. Rivera, K. L. Seyler, H. Yu, J. R. Schaibley, J. Yan, D. G. Mandrus, W. Yao and X. Xu, *Science*, 2016, **351**, 688–691.
15 L. A. Jauregui, A. Y. Joe, K. Pistunova, D. S. Wild, A. A. High, Y. Zho, G. Scuri, K. D. Greve, A. Sushko, C. Yu, T. Taniguchi, K. Watanabe, D. J. Needleman, M. D. Lukin, H. Park and P. Kim, *Science*, 2019, **366**, 870–875.
16 J. Kiemle, F. Sigger, M. Lorke, B. Miller, K. Watanabe, T. Taniguchi, A. Holleitner and U. Wurstbauer, *Phys. Rev. B*, 2020, **101**, 121404.
17 G. Scuri, T. I. Andersen, Y. Zhou, D. S. Wild, J. Sung, R. J. Gelly, D. Bérubé, H. Heo, L. Shao, A. Y. Joe, A. M. Mier Valdivia, T. Taniguchi, K. Watanabe, M. Lončar, P. Kim, M. D. Lukin and H. Park, *Phys. Rev. Lett.*, 2020, **124**, 217403.
18 Y. Jiang, S. Chen, W. Zheng, B. Zheng and A. Pan, *Light: Sci. Appl.*, 2021, **10**, 72.
19 C. Robert, D. Lagarde, F. Cadiz, G. Wang, B. Lassagne, T. Amand, A. Balocchi, P. Renucci, S. Tongay, B. Urbaszek and X. Marie, *Phys. Rev. B*, 2016, **93**, 205423.
20 H. H. Fang, B. Han, C. Robert, M. A. Semina, D. Lagarde, E. Courtade, T. Taniguchi, K. Watanabe, T. Amand, B. Urbaszek, M. M. Glazov and X. Marie, *Phys. Rev. Lett.*, 2019, **123**, 067401.
21 M. Yang, L. Ren, C. Robert, D. V. Tuan, L. Lombez, B. Urbaszek, X. Marie and H. Dery, *Phys. Rev. B*, 2022, **105**, 085302.
22 P. Nagler, G. Plechinger, M. V. Ballottin, A. Mitioglu, S. Meier, N. Paradiso, C. Strunk, A. Chernikov, P. C. M. Christianen, C. Schüller and T. Korn, *2D Mater.*, 2017, **4**, 025112.
23 Q. Tan, A. Rasmita, Z. Zhang, H. Cai, X. Cai, X. Dai, K. Watanabe, T. Taniguchi, A. H. MacDonald and W. Gao, *Nat. Mater.*, 2023, **22**, 605–611.

24 S. Chatterjee, M. Dandu, P. Dasika, R. Biswas, S. Das, K. Watanabe, T. Taniguchi, V. Raghunathan and K. Majumdar, *Nat. Commun.*, 2023, **14**, 4679.
25 N. Zhang, A. Surrente, M. Baranowski, D. K. Maude, P. Gant, A. Castellanos-Gomez and P. Plochocka, *Nano Lett.*, 2018, **18**, 751–757.
26 J. Shi, Y. Li, Z. Zhang, W. Feng, Q. Wang, S. Ren, J. Zhang, W. Du, X. Wu, X. Sui, Y. Mi, R. Wang, Y. Sun, L. Zhang, X. Qiu, J. Lu, C. Shen, Y. Zhang, Q. Zhang and X. Liu, *ACS Photonics*, 2019, **6**, 3082–3091.
27 M. Dandu, G. Gupta, P. Dasika, K. Watanabe, T. Taniguchi and K. Majumdar, *ACS Nano*, 2022, **16**, 8983–8992.
28 Y. Meng, T. Wang, C. Jin, Z. Li, S. Miao, Z. Lian, T. Taniguchi, K. Watanabe, F. Song and S. Shi, *Nat. Commun.*, 2020, **11**, 2640.
29 C. Ge, L. Huang, D. Zhang, Q. Tong, X. Zhu, X. Wang and A. Pan, *AIP Adv.*, 2023, **13**, 115101.
30 K. Wang, B. Huang, M. Tian, F. Ceballos, M. Lin, M. Mahjouri-Samani, A. Boulesbaa, A. A. Puretzky, C. M. Rouleau, M. Yoon, H. Zhao, K. Xiao, G. Duscher and D. B. Geohegan, *ACS Nano*, 2016, **10**, 6612–6622.
31 Y. Yoon, Z. Zhang, R. Qi, A. Y. Joe, R. Sailus, K. Watanabe, T. Taniguchi, S. Tongay and F. Wang, *Nano Lett.*, 2022, **22**, 10140–10146.
32 V. R. Policht, H. Mittenzwey, O. Dogadov, M. Katzer, A. Villa, Q. Li, B. Kaiser, A. M. Ross, F. Scotognella, X. Zhu, A. Knorr, M. Selig, G. Cerullo and S. D. Conte, *Nat. Commun.*, 2023, **14**, 7273.
33 B. Zhu, X. Chen and X. Cui, *Sci. Rep.*, 2015, **5**, 9218.
34 C. Jin, J. Kim, M. I. B. Utama, E. C. Regan, H. Kleemann, H. Cai, Y. Shen, M. J. Shinner, A. Sengupta, K. Watanabe, T. Taniguchi, S. Tongay, A. Zettl and F. Wang, *Science*, 2018, **360**, 893–896.
35 J. Chen, X. Yue, Y. Shan, H. Wang, J. Han, H. Wang, C. Sheng, L. Hu, R. Liu, W. Yang, Z. Qiu and C. Cong, *RSC Adv.*, 2023, **13**, 18099–18107.
36 D. Lien, S. Z. Uddin, M. Yeh, M. Amani, H. Kim, J. W. Ager III, E. Yablonovitch and A. Javey, *Science*, 2019, **364**, 468–471.
37 A. Wang, W. Yao, Z. Yang, D. Zheng, S. Lin, Y. Shi, D. Li and F. Wang, *Nanoscale*, 2023, **15**, 19777–19783.
38 V. R. Policht, M. Russo, F. Liu, C. Trovatello, M. Maiuri, Y. Bai, X. Zhu, S. D. Conte and G. Cerullo, *Nano Lett.*, 2021, **21**, 4738–4743.